Computers and Geotechnics 68 (2015) 196–207

Contents lists available at ScienceDirect

Computers and Geotechnics

journal homepage: www.elsevier.com/locate/compgeo

Research Paper

Evaluation of hydraulic parameters from pumping tests in multi-aquifers with vertical leakage in Tianjin

Shui-Long Shen [a,*], Yong-Xia Wu [a,*], Ye-Shuang Xu [a], Takenori Hino [b,c], Huai-Na Wu [a]

[a] State Key Laboratory of Ocean Engineering, Department of Civil Engineering, Shanghai Jiao Tong University, Shanghai 200240, China
[b] Department of Civil Engineering, Shanghai Jiao Tong University, Shanghai 200240, China
[c] Institute of Lowland and Marine Research, Saga University, Japan

ARTICLE INFO

Article history:
Received 8 December 2014
Received in revised form 24 March 2015
Accepted 25 March 2015
Available online 2 May 2015

Keywords:
Pumping test
Analytical method
Numerical method
Hydrogeological parameters

ABSTRACT

This paper presents a case history of behaviour during a series of pumping tests in an alternated multi-aquifer-aquitard system in a foundation pit in Tianjin, China. The test site is located at Tianjin Railway Station, which is in the downtown area and is surrounded by many buildings. The groundwater system at the test site is composed of a phreatic aquifer and three confined aquifers. Four groups of single well pumping tests were conducted in each aquifer to obtain the hydrogeological parameters of the aquifers and investigate the hydraulic connection among the aquifers. Test results show that there is hydraulic connection among the upper 3 aquifers. Moreover, both analytical and numerical methods were employed to analyse the hydrogeological parameters. The analytical solution was obtained for the phreatic aquifer using the Dupuit equation, and the Cooper–Jacob method was conducted for the confined aquifers. The numerical simulation was performed using a finite element method (FEM). The results illustrate that the numerical method gives more reliable results than the analytical method does. The numerical simulation considers the anisotropic characteristic of soils, and the hydrogeological parameters of all of the soils can be calculated. The analytical solution, however, may be influenced by wellbore storage or by the leakage effect of the aquitards, and it only gives the parameters of the aquifer where the pumping tests were performed.

1. Introduction

Soft Quaternary deposits of large thickness are distributed in the coastal regions of China under different palaeoclimatic and sedimentary (marine or terrestrial) environments, forming an alternated multi-aquifer aquitard system (MAAS) with the characteristic of a very high groundwater head [4,47,50]. When excavation pits are located in this type of soft deposit, dewatering is conducted to ensure excavation safety [34,38,45]. In general, dewatering may last for months or even more than one year, which may cause ground settlement [5–7,35,40,42]. In the analysis of excavation dewatering, understanding the hydrogeological parameters, such as the hydraulic conductivity (k), transmissivity (T), and storage coefficient (S), is helpful in reducing the settlement caused by dewatering.

There are three common ways to ascertain the hydrogeological characteristics of soils: predicting methods [10,12,28], laboratory tests [8,25,26] and field tests [11,16,32]. Among these, field tests, such as pumping tests and slug tests, are the most widely used. Slug tests are primarily used in weak aquifers, where it is difficult to draw groundwater continuously, and pumping tests are commonly used in aquifers, where groundwater can be drawn easily. Generally, an analytical method for non-steady flow has been used to obtain hydrogeological parameters by matching observed drawdown data [3,13,14,18,19,37,43]. In recent years, back calculation through a numerical method has become more widely used, particularly in complicated geological environments [20,22–24,27,46].

This paper presents a field case study of pumping tests conducted in Tianjin, China. Both analytical and numerical methods are employed to obtain the hydrogeological parameters, and the results from the two methods are compared.

2. Site conditions

The Tianjin transportation hub project is located in the Hedong district of Tianjin and includes the traffic square behind Tianjin

* Corresponding authors. Tel.: +86 21 3420 4301; fax: +86 21 6419 1030 (S.-L. Shen).
E-mail addresses: slshen@sjtu.edu.cn (S.-L. Shen), wxia2011@sjtu.edu.cn (Y.-X. Wu), xuyeshuang@sjtu.edu.cn (Y.-S. Xu), hino@ilt.saga-u.ac.jp (T. Hino), wu-hn@sjtu.edu.cn (H.-N. Wu).

http://dx.doi.org/10.1016/j.compgeo.2015.03.011
0266-352X/

Railway Station, the landscaped square in front of Tianjin Station, and the related municipal works. The traffic square is the transfer hub for metro lines 2, 3, and 9, Jinjing Intercity Railway and China Railway. Metro line 2 is parallel to metro line 9 from east to west and crosses metro line 3 below the traffic square. The construction site is 400 m from the Haihe River. Fig. 1 presents the site plan of the transfer hub project. There are many buildings around the excavation pit. The excavation pit consists of three sections (sections I, II, and III). It is one of the largest and deepest excavations ever constructed in Tianjin. The depth of the excavation varies from 23.0 m to 32.5 m. To investigate the groundwater conditions at the project site, several single-well pumping tests were performed in the planning square. The test site was approximately 315 m from the excavation (see Fig. 1).

3. Engineering geology and hydrogeology

3.1. Geological conditions

The elevation at the test site is 2.3–2.4 m above sea level. Fig. 2 shows the soil profile and properties at the construction site. As observed in Fig. 2, the investigation area is characterised as a marine–terrestrial zone with silty sand, silt and silty clay. The first layer is uncontrolled fill (artificial layer) in the upper 2.6 m below the ground surface, followed by silty clay and silt to a depth of 12.6 m. The next layer is silty clay extending to a depth of 20.5 m, which is underlain by silt and silty sand to a depth of 32.1 m. These layers are underlain by silty clay with some silt to a depth of 44.4 m. The subjacent layer is silt to a depth of 47.2 m. Under the silt, silty clay is present at the site, to a depth of 64.0 m. The following layer is silty sand to a depth of 68.0 m. Beneath this layer is a layer of silty clay until the termination depth of 80 m.

The soil properties along the depth were established through a series of laboratory tests. The grain size distribution indicates that the silt content of the silty clay and silt is relatively high, at approximately 78%. The initial void ratio, e_0, was determined based on the soil's physical properties from the laboratory tests. The water contents are generally close to the liquid limit, apart from that of silty clay, whereas the plasticity index of the silty clay is approximately 19%. The compression index, C_c, was obtained from laboratory oedometer tests. For the layers from the ground surface to 15 m deep, the compression index, C_c, ranges from 0.2 to 0.4, and for the soil layers at depths of more than 20 m, C_c, ranges from 0.1 to 0.2.

3.2. Hydrogeology

The types of groundwater are phreatic water and confined water. There are one phreatic aquifer (referred to as Aq0) and three confined aquifers (referred to as AqI, AqII, and AqIII). The aquifers are separated by three aquitards (referred to as AdI, AdII, and AdIII). The values of hydraulic conductivity k_h and k_v that are plotted in Fig. 2 were obtained from laboratory oedometer tests using soil samples extracted in both horizontal and vertical directions, respectively. Table 1 lists the measured values of k_h, k_v, and k_h/k_v, which shows that k_h/k_v varied from 1.5 to 5.8.

Aq0 is primarily composed of silt with a thickness of 7.3 m. In this article, the ground surface is taken as the reference datum; the water level of the phreatic aquifer is −1.90 to −1.97 m. AqI is mainly composed of silt and silty sand. The average thickness of the sand is 5.0 m. The water level of AqI is −2.79 to −2.84 m. AqII is mainly composed of silt with an average thickness of 2.0 m. The continuity of this layer is not good in the horizontal direction. The water level of AqII is −3.07 to −3.38 m. AqIII is mainly composed of silty sand with an average thickness of 4.0 m. The water level of AqIII is −12.25 to −12.35 m.

4. Pumping tests

4.1. Well installation

Pumping tests were performed between March 16, 2006, and April 4, 2006 [51]. Fig. 3 shows a plan layout of the wells. There are four pumping wells (labelled W1–W4) and ten monitoring wells. The monitoring wells for pumping well W1 were P1-1 and P1-2, for pumping well W2 were P2-1 to P2-3, for pumping well W3 were P3-1 to P3-3, and for pumping well W4 were P4-1 and P4-2. The distance between wells W1 and P1-1 and P1-2 was 3.35 m and 7.90 m, that between wells W2 and P2-1, P2-2 and P2-3 was 3.85 m, 8.95 m and 19.75 m, that between wells W3 and P3-1, P3-2 and P3-3 was 4.00 m, 9.10 m and 19.90 m, and that between wells W4 and P4-1 and P4-2 was 7.91 m and 12.31 m, respectively. Fig. 4 plots the structure of the wells. The pumping wells W1–W4 were installed in Aq0 to AqIII at depths of 18 m, 35 m, 50 m and 71 m, respectively. The four wells were fully penetrating wells with an internal radius of 300 mm and an external radius of 610 mm. The screens of the pumping wells were 11 m long in Aq0, 9 m long in AqI, 4 m long in AqII, and 7 m long in AqIII. The monitoring wells had an internal radius of 219 mm

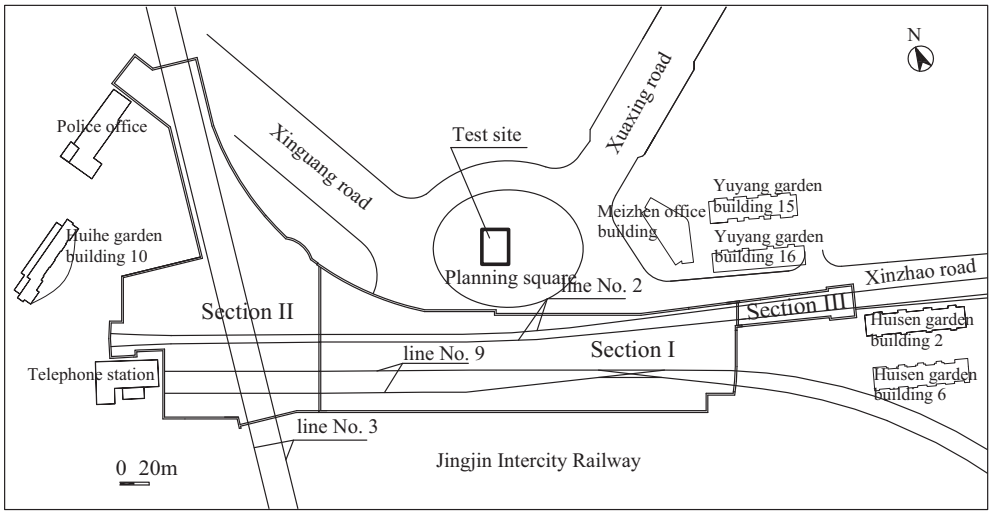

Fig. 1. Plan view of the construction site.

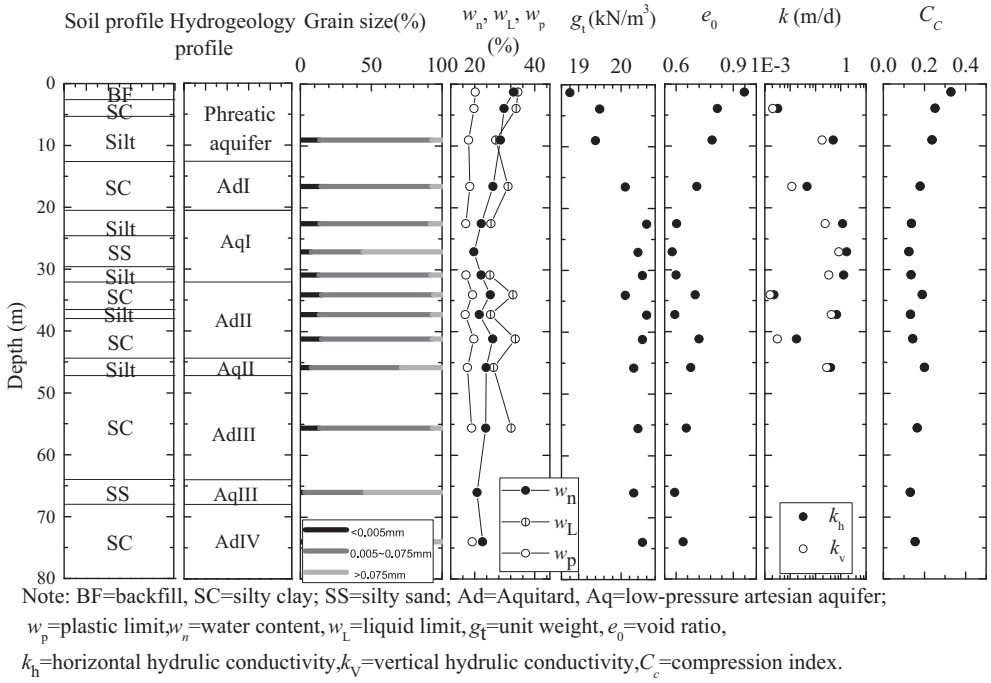

Fig. 2. Soil profile and properties at the construction site.

Table 1
Hydraulic conductivities from laboratory tests.

Soil strata	k_h (m/d)	k_v (m/d)	k_h/k_v
Silty clay	3.28E−05	2.07E−05	1.58
Silt	5.01E−03	1.86E−03	2.69
Silty clay	4.67E−04	1.18E−04	3.96
Silt	1.20E−02	2.42E−03	4.96
Silty sand	1.73E−02	8.44E−03	2.05
Silt	1.30E−02	3.40E−03	3.82
Silty clay	2.33E−05	1.64E−05	1.42
Silt	6.91E−03	4.32E−03	1.60
Silty clay	1.81E−04	3.15E−05	5.74
Silt	3.97E−03	2.80E−03	1.42

Note: k_h = horizontal hydraulic conductivity; k_v = vertical hydraulic conductivity.

and an external radius of 400 mm. The depths and screens of the monitoring wells and the pumping wells were the same, except for P2-1 to P2-3, which had a depth of 33 m and 7 m long screens.

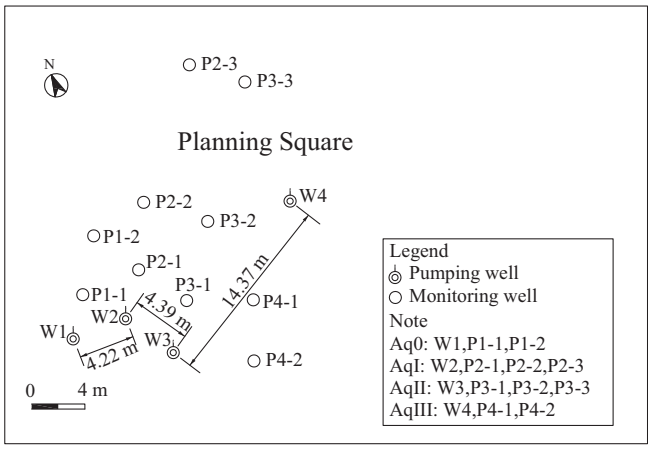

Fig. 3. Plan view of the wells.

4.2. Field quality control of boring well

To prevent leakage along the well wall, both during boring and when installing the casing in aquitards, wells outside the steel pipes were sealed with a bentonite clay ball to prevent groundwater from adjacent aquifers coming into the wells. When bentonite clay meets water, it becomes a slurry and swells. The hydraulic conductivity of bentonite slurry is much lower than that of the original aquitard soil. Swelling of the bentonite slurry can efficiently seal the surface of steel wells. This seal method for the quality control of boring wells was established by Chinese Construction Code [29], and its effectiveness can be verified from the pumping test of well W4, which is presented below. For the screen section in the aquifer, wells were filled with 0.25–0.5 mm diameter quartz sand to ensure easy groundwater flow.

4.3. Pumping tests

The pumping tests were performed from the commencement of pumping until the end of the recovery periods. During the pumping tests, the water level was measured in the 4 pumping wells and the 10 monitoring wells. Table 2 shows the detailed process of the test cases. As observed in the table, the pumping tests were conducted on different scales in each aquifer; the drawdown in the pumping wells for each aquifer was also recorded on different scales. The pumping period ranged from 1200 min to 3540 min, the recovery time was from 1260 min to 4320 min, and the discharge rate was from 14.69 to 295.92 m^3/d.

5. Results and analyses

5.1. Test results

Fig. 5 presents the variation of the groundwater level measured in the monitoring wells during the pumping tests. Within each pumping test, the change in the groundwater head followed a similar trend. At the beginning of a pumping test, the groundwater

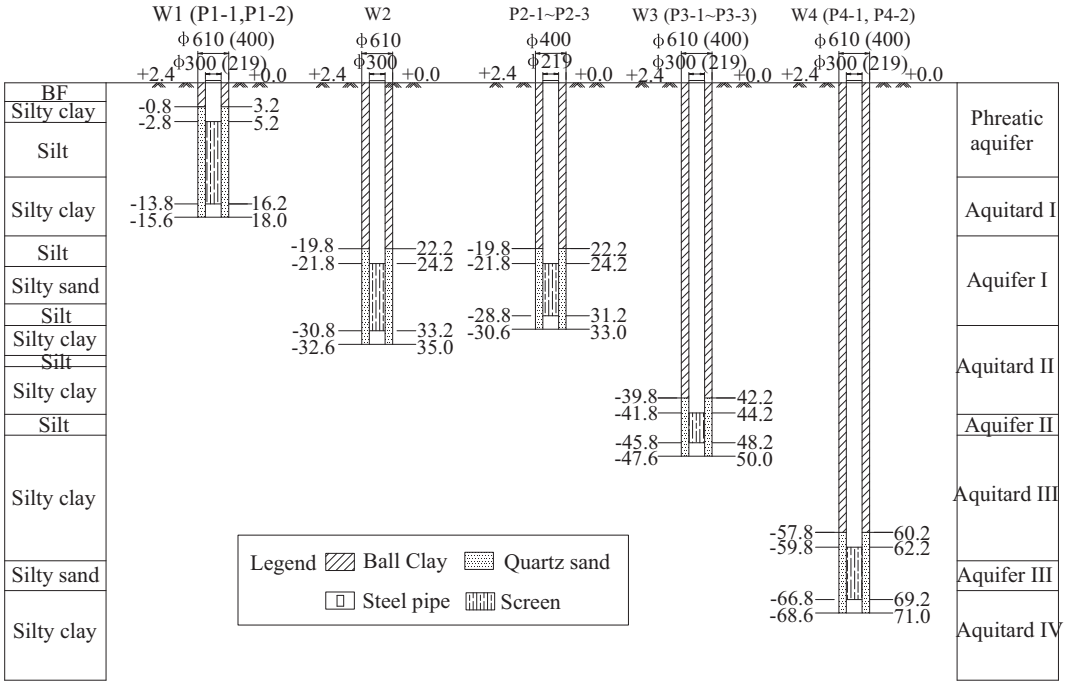

Fig. 4. Structure of the wells.

Table 2
Process of the pumping tests.

Aquifer	Pumping well	Drawdown scale	h_0 (m)	s_w (m)	t_0	t_e	t_p (min)	t_r (min)	Q (m^3/d)
Aq0	W1	Full	1.70	13.00	10:00 30 Mar.	2:30 1 Apr.	2430	2520	14.69
AqI	W2	Small	2.52	4.41	10:30 21 Mar.	22:30 22 Mar.	2160	/	102.96
		Intermediate		12.58	22:30 22 Mar.	9:30 25 Mar.	3540	4320	234.48
		Large	2.52	19.28	13:00 16 Mar.	9:00 17 Mar.	1200	1980	295.92
AqII	W3	Full	3.12	40.01	22:30 18 Mar.	15:00 20 Mar.	2430	3510	28.13
AqIII	W4	Intermediate	11.95	26.97	14:30 25 Mar.	10:30 27 Mar.	2640	/	86.40
		Large		40.20	10:30 27 Mar.	10:30 29 Mar.	2880	1260	126.24
		Small	12.42	14.74	18:00 1 Apr.	22:00 2 Apr.	1680	2160	52.80

Note: h_0 = depth of static water head; s_w = drawdown of pumping well; t_0 = starting time; t_e = ending time; t_p = pumping time; t_r = recovery time; Q = discharge.

head declined rapidly at first and then decreased at a slower rate until it reached a steady level. When the pump was shut down, the groundwater head recovered quickly. In the W1 pumping test, the maximum drawdown of AqI monitored in P2-1 was 0.125 m, and the groundwater level of AqII did not change when the drawdown of pumping well W1 was 13.00 m. In the W2 pumping test, the maximum drawdown of Aq0 monitored in P1-1 was 1.1 m, and the maximum drawdown of AqII monitored in P3-1 was 0.3 m when the drawdown of pumping well W2 was 12.58 m. Although the pumping rate of W3 was only 28.13 m^3/d, the groundwater level of AqII declined sharply, whereas the groundwater levels of AqI and AqIII did not change. In addition, the pumping tests in AqIII illustrate that there was no variation in the groundwater level in Aq0, AqI, and AqII when pumping groundwater from AqIII.

5.2. Analyses

The static groundwater level in Tianjin became uniform a long time ago. However, at present, the initial water level in each aquifer is different, particularly the water level in AqIII. This has occurred because groundwater has been exploited from deep aquifers, e.g., AqIII, for a long time, which has led to a decline in the AqIII water level. Because the hydraulic conductivity of AdIII is poor, water levels in Aq0, AqI and AqII were not affected during pumping in Aquifer III. However, the groundwater in shallow aquifers (AqI and AqII) was withdrawn during the construction of a foundation pit, which caused the difference of the initial water level before pumping in this project. However, this difference is small among Aq0, AqI, and AqII, with only a 0.82 m difference between Aq0 and AqI and a 0.6 m difference between AqI and AqII. The thicknesses of aquitard I and II are 7.9 m and 12.3 m, respectively. Thus, the hydraulic gradients between Aq0 and AqI and between AqI and AqII are only 0.104 and 0.049. According to Bear [1], in the application of Darcy's law of saturated flow through porous media, there exists a minimum (or initial) gradient J_0, below which there is very little flow. Fig. 6 illustrates the concept of the threshed hydraulic gradient J_0 to trigger seepage. Bear [1] commented that "this phenomenon to the rheological non-Newtonian behaviour of the water. Some authors attribute J_0 to the fact that the streaming potential generated by the flow, particularly in fine-grained soils, can produce small counter-currents along the pore walls in a direction opposite that of the main flow. This, at least in fine-grained cohesive soils, may result in no flow before the threshold gradient J_0 is exceeded".

To estimate the triggering hydraulic gradient for AdI and AdII, the drawdown in the non-pumping aquifer and the "apparent" hydraulic gradient between aquifers of one aquitard were plotted. We use a new term, "apparent hydraulic gradient", for this

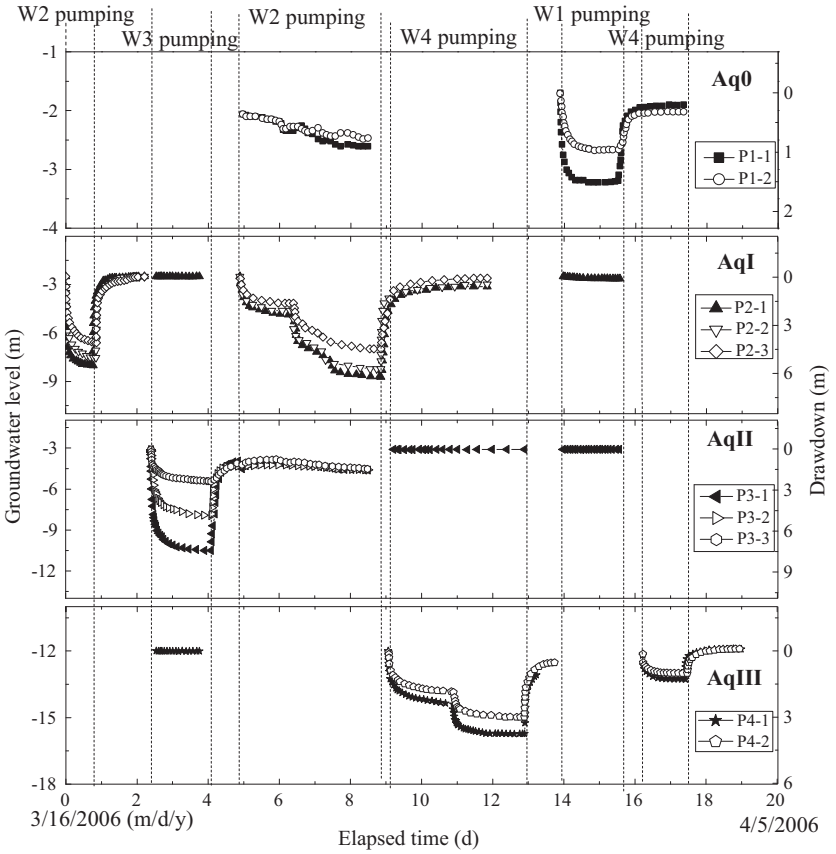

Fig. 5. Variation in the groundwater level measured in the monitoring wells during pumping tests.

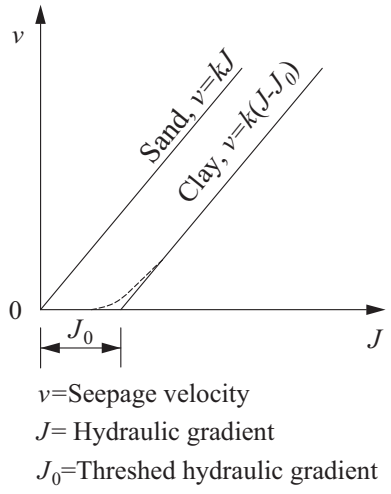

Fig. 6. Relationship between seepage velocity and hydraulic gradient (created from [1]).

estimation. Because the monitoring wells in different aquifers are not in the same position, a hydraulic gradient is derived from the head differences of the monitoring wells in different aquifers. The apparent hydraulic gradient is defined as follows:

$$h_a = \frac{L_{aqupper} - L_{aqlower}}{H_{ad}} \quad (1)$$

where h_a = 'apparent' hydraulic gradient; H_{ad} = thickness of the aquitard; L = groundwater head in the aquifer; aqupper = upper aquifer; and aqlower = lower aquifer.

Fig. 7 shows the relationship between the drawdown in non-pumping aquifers and the apparent hydraulic gradient. From this figure, we can roughly estimate the triggering hydraulic gradient. For AdI, when pumping was performed in AqI (the lower aquifer of AdI), the triggering incremental apparent hydraulic gradient was $\Delta h_a = 0.21$, whereas when pumping was performed in Aq0, the upper aquifer of AdI, the triggering incremental apparent hydraulic gradient was $\Delta h_a = 0.104$, which is lower than that pumping in AqI. For AdII, as shown in Fig. 7b, when pumping was performed in AqII, the drawdown in AqI was minimal and the apparent hydraulic gradient h_a reached 0.3, whereas when pumping was performed in AqI (the upper aquifer of AdII), the triggering incremental apparent hydraulic gradient was $\Delta h_a = 0.24$. The reason for this difference is not clear but may be due to (i) the hydraulic gradients not being accurate and (ii) the field conditions being complex.

Thus, it is difficult to estimate the threshold hydraulic gradient accurately from the field test data; however, we can give approximate values. For AdI J_0, the range is from 0.1 to 0.2, and for AdII, J_0 ranges from 0.2 to 0.3. To clarify this problem, further well control tests should be conducted.

6. Analyses of aquifer parameters

6.1. Hydraulic conductivity and storage coefficient

For comparison, full-scale drawdown of Aq0 and AqII and intermediate-scale drawdown of AqI and AqIII were selected to calculate the parameters of Aq0, AqI, AqII, and AqIII.

6.1.1. Aq0: Dupuit equation

The Aq0 pumping test was analysed assuming phreatic aquifer flow using the Dupuit equation [15]:

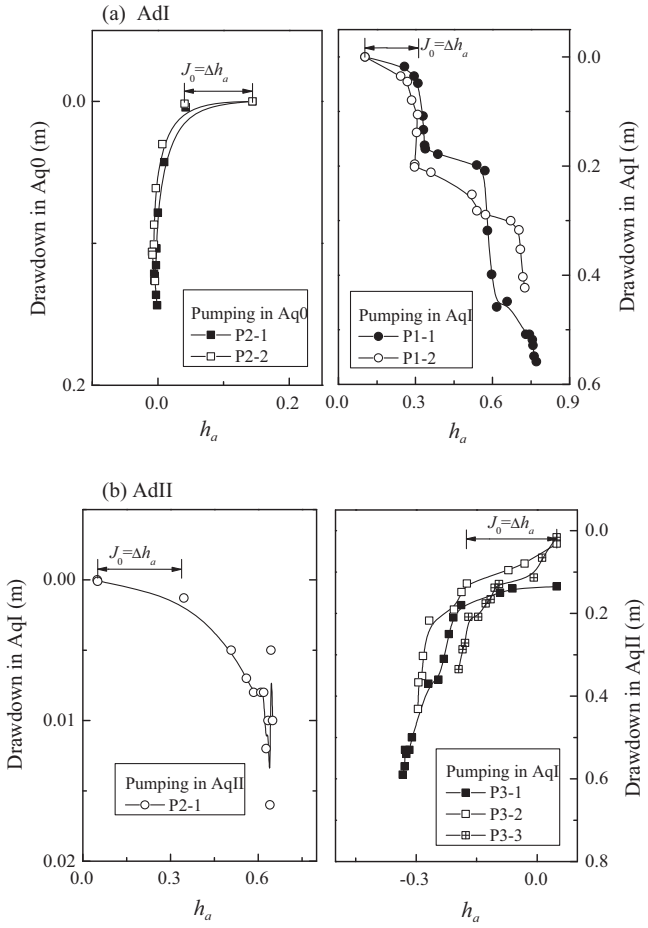

Fig. 7. Relationship between drawdown in non-pumping aquifers and the apparent hydraulic gradient.

$$k = \frac{0.732Q\lg(r_2/r_1)}{(2H - s_1 - s_2)(s_1 - s_2)} \tag{2}$$

where H is the average thickness of Aq0 (9.6 m), r is the distance from the monitoring well to the pumping well, s is the drawdown (s_1 = 1.52 m at r_1 = 3.35 m and s_2 = 0.97 m at r_2 = 7.9 m), and Q is the constant pumping rate (14.69 m^3/d). Substituting into Eq. (1), this gives k = 0.44 m/d.

6.1.2. AqI, AqII and AqIII: Cooper–Jacob, s versus log t

For confined aquifers, the semi-log graph derived by Cooper and Jacob [14] was used to calculate the hydrogeological parameters. Three detailed graphs of s versus log t are shown in Fig. 8.

The transmissivity, T, is given by the slope, Δs, of the linear portion of the graph as

$$T = \frac{2.30Q}{4\pi\Delta s} \tag{3}$$

and the storage coefficient, S, is given by the time intercept, t_0, as

$$S = \frac{2.25Tt_0}{r^2} \tag{4}$$

where r is the distance between the observational well and pumping well. With the given values of Δs, t_0 and r, T and S can be determined based on Eqs. (3) and (4).

The hydraulic conductivity, k, is obtained from the transmissivity, as

$$k = \frac{T}{M} \tag{5}$$

where M is the thickness of the confined aquifer.

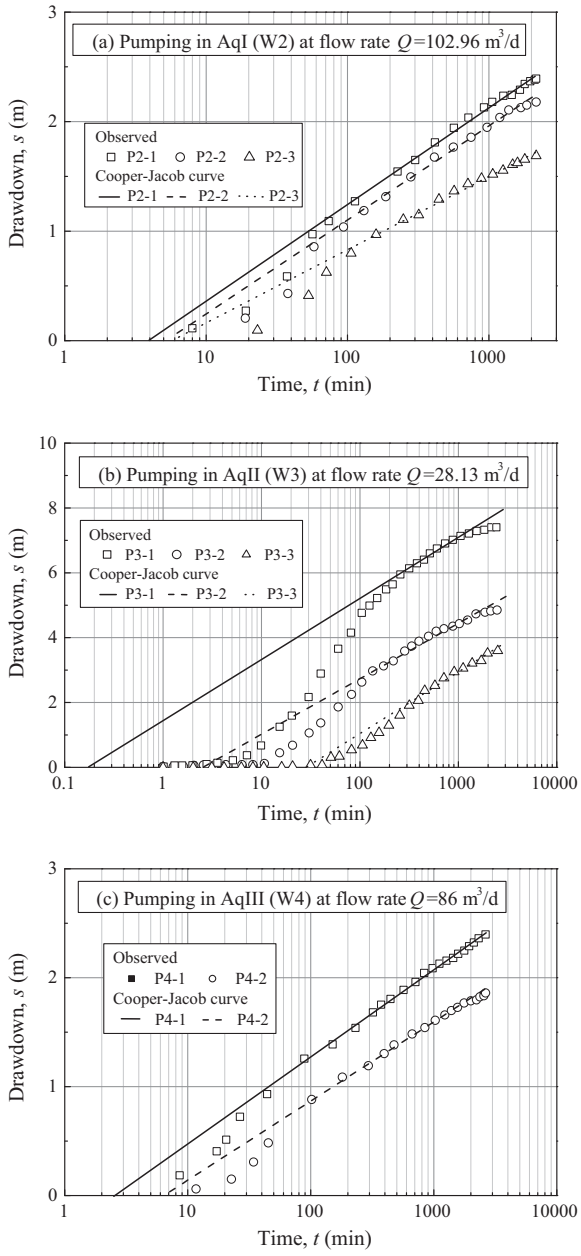

Fig. 8. Graph of the drawdown versus logarithmic time (log t) for the pumping test results.

Table 3 shows the values for the hydrogeological parameters obtained from Eqs. (3)–(5) based on the pumping test data. The average S values of AqI, AqII and AqIII are 6.89×10^{-4}, 2.11×10^{-4} and 3.00×10^{-4}, respectively. The average hydraulic conductivity k values of AqI, AqII and AqIII are 4.94 m/d, 1.38 m/d and 3.84 m/d, respectively. Among these, the k value of AqI is the highest because it is primarily composed of silty sand, and the k value of AqII is the lowest because it is composed of silt.

6.2. Influence radius

Because steady flow does not exist in an infinite aquifer, the influence radius of the well, R, is defined as the distance from the pumping well to a place where drawdown can be neglected. If the values of k and the drawdown of the pumping well, s_w, are known, R can be calculated from empirical formulae [2].

Table 3
Hydrogeological parameters from analytical method.

Aquifer	Monitoring well	r (m)	T (m^2/d)	S	k (m/d)	Average T (m^2/d)	Average S	Average k (m/d)
Aq0	P1-1	3.35		/	0.44	/	/	0.44
	P1-2	7.90			0.44			
AqI	P2-1	3.85	23.56	7.45E−3	4.71	24.71	6.89E−4	4.94
	P2-2	8.95	22.44	2.23E−3	4.49			
	P2-3	19.75	28.12	6.53E−4	5.62			
AqII	P3-1	4.00	2.71	1.85E−4	1.35	2.76	2.11E−4	1.38
	P3-2	9.10	2.92	1.32E−4	1.46			
	P3-3	19.90	2.66	3.16E−4	1.33			
AqIII	P4-1	7.91	17.59	1.01E−3	3.47	19.35	3.00E−4	3.84
	P4-2	12.31	21.12	1.39E−3	4.22			

Note: r = distance from monitoring well to pumping well; T = transmissivity; S = storage coefficient; k = hydraulic conductivity.

However, the observed drawdown is composed of two parts: s_w and well loss [2]. Because well loss is related to well quality, screens and gravel-filling, it is difficult to obtain an accurate value for s_w. In this case, the drawdowns of the observation wells were monitored such that R is calculated based on observation data. For Aq0 and AqIII, there are two monitoring wells for each pumping test, and an approximate method is used. For AqI and AqII, there are three monitoring wells for each pumping test, and a graphical method is applied.

6.2.1. Aq0 and AqIII: approximate method

According to the Thiem equation, the influence radius of the well can be calculated from the following equations.

For a confined aquifer:

$$\lg R = \frac{s_1 \lg r_2 - s_2 \lg r_1}{s_1 - s_2} \tag{6}$$

For a phreatic aquifer:

$$\lg R = \frac{s_1(2H - s_1)\lg r_2 - s_2(2H - s_2)\lg r_1}{(s_1 - s_2)(2H - s_1 - s_2)} \tag{7}$$

where s_1 and s_2 = drawdown of monitoring wells, r_1 and r_2 = distance from monitoring wells to pumping well, and H = initial thickness of the phreatic aquifer.

With s, r, and H, Eqs. (6) and (7) give values of R. The values of the influence radius are 48 m for W1 in Aq0, and 18 m, 20 m and 72 m for W4 in AqIII during small-, intermediate- and large-scale tests, respectively.

6.2.2. AqI and AqII: graphical method

The influence of the radius can be obtained by drawing a tendency chart of s versus $\log r$. The intersection point of the curve and the straight line of $s = 0$ is the influence radius. Fig. 9 shows the curve of s versus $\log r$ and the corresponding trend line of each pumping test. The values of the influence radius are 220 m and 480 m for W2 in AqI during the small- and intermediate-scale tests, respectively, and 95 m for W3 in AqII.

7. Numerical analysis

7.1. Numerical model

Based on Darcy's law and the principle of continuity, the governing equation for groundwater seepage in saturated media is expressed as follows [2,40,41]:

$$\frac{\partial}{\partial x_i}\left(K_{ij}\frac{\partial h}{\partial x_j}\right) - Q = S_S\frac{\partial h}{\partial t} \tag{8}$$

where K_{ij} = hydraulic conductivity, h = hydraulic head, Q = external source/sink flux, S_s = specific storage, and t = time.

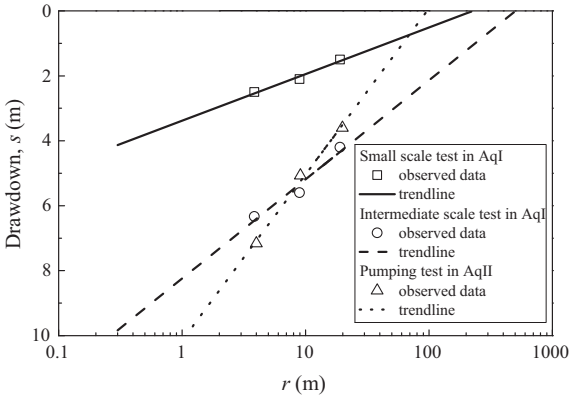

Fig. 9. Curve of the drawdown versus influence radius r and the corresponding trend-line.

The initial condition is expressed as

$$h(x,y,z,t)|_{t=t_0} = h_0(x,y,z) \tag{9}$$

where $h_0(x, y, z)$ = initial hydraulic head at point (x, y, z).

The boundary conditions are expressed as

$$h(x,y,z,t)|_{\Gamma_1} = h_1(x,y,z,t) \tag{10}$$

$$\left(k_{xx}\frac{\partial h}{\partial n_x} + k_{yy}\frac{\partial h}{\partial n_y} + k_{zz}\frac{\partial h}{\partial n_z}\right)\Big|_{\Gamma_2} = q(x,y,z,t) \tag{11}$$

where $h_1(x, y, z, t)$ = constant head on boundary Γ_1; n_x, n_y, n_z = unit normal vector on boundary Γ_2 along the x, y and z directions; $q(x, y, z, t)$ = lateral recharge per unit area on boundary Γ_2; Γ_1 = first type of boundary condition; and Γ_2 = second type of boundary condition.

7.1.1. Calculation range

According to the calculation result of the influence radius, the numerical simulation range extends more than 480 m from well W2. The whole calculation area is 1000 m by 1000 m in-plane. Fig. 10 presents the 3D finite element mesh [40,41]. The finite element mesh in the horizontal direction is dense at the test site, and it gradually becomes sparse from the test site outwards (see Fig. 11). There are 76 rows and 70 columns. The engineering geology includes 14 strata and is represented by 17 layers. To determine the effect of the size of the mesh on the numerical results, four mesh schemes were examined. Among them, the mesh size in the pumping test site was small and gradually enlarged to the outside. The difference in the first three schemes is the largest aspect ratio of the elements. The four schemes are as follows: (i) the present mesh size,

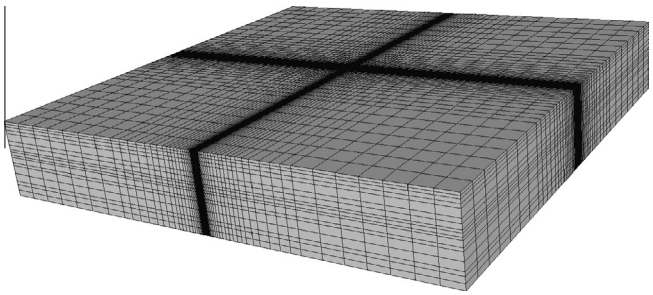

Fig. 10. Three-dimensional (3D) finite element mesh.

i.e., the mesh size in the pumping/monitoring wells area is 1 m × 1 m, and the largest aspect ratio is 40:1; (ii) the largest aspect ratio is 20:1; (iii) the largest aspect ratio is 10:1; and (iv) the mesh size in the pumping/monitoring wells area is 2 m × 2 m and the largest aspect ratio is 40:1. The results show that in the considered region (pumping and monitoring areas), the maximum difference between mesh schemes (i) and (iv) is approximately 19%, and the difference among mesh schemes (i), (ii) and (iii) is less than 1.0% because the largest aspect ratio element is far from the test site. Thus, the adopted scheme for mesh size is sufficiently accurate for the research area. Moreover, the adopted mesh scheme is the most cost-effective and time-saving scheme.

7.1.2. Initial/boundary conditions

The initial hydraulic head of the phreatic water is set at 1.7 m below the ground surface, and that of AqI, AqII, and AqIII are set at 2.5 m, 3.1 m and 12 m below the ground surface, respectively. The boundary condition is constant hydraulic head, which is equal to the initial hydraulic head. The only source and sink term is the pumping wells. Full-scale tests in Aq0, AqII, small- and intermediate-scale tests in AqI, and intermediate- and large-scale tests in AqIII are selected to calculate the parameters. Table 2 shows the rates of groundwater extraction per day.

7.1.3. Soil parameters

Table 4 shows the final values of k_h, k_v and S_s for each layer. The initial values of k_h, k_v and S_s for the aquifers are based on observed data from single well pumping tests and an analytical method. The horizontal hydraulic conductivity k_h is selected in the range of 2–3 times the vertical hydraulic conductivity k_v, based on the oedometer test results, as shown in Table 1, the experience of the authors [39,48,49,56] and from the literature [52–55]. The k values of silty clay are based on the oedometer tests to determine the soil properties. Because there is silt in the sand layer of AqI and silty clay in the silt layer of AqII, AqI and AqII were divided into two parameter zones, and different values were assigned. The distribution of the values can be observed in Fig. 13. The values, including assumed values for the aquitards, were modified by trial and error to minimise the differences between the calculated values and the observed values as much as possible.

The parameters were calculated by the following steps:

Step 1: The initial values of k_h, k_v and S_s for the aquifers and aquitards were determined based on the available data of the geological investigation code [30]. Because the drill-hole data was just in and around the test site, the ranges of silt in the sand layer of AqI and the silty clay in the silt layer of AqII were estimated using the method in the code [30].
Step 2: The numerical values were compared with the observed values. If there was a significant difference between them, the parameters were changed manually. For silt in the sand layer of AqI and silty clay in the silt layer of AqII, the range was also adjusted.
Step 3: Repeat step 2 continuously until the differences between calculated values and observed values are sufficiently small.

7.2. Results

Fig. 12 shows a comparison between the observed and calculated drawdown of the monitoring wells in each aquifer. In this figure, the numerical results match the observed results for most of the observational wells. However, for observational well P2-1, there are some discrepancies between the observed and simulated results because the monitoring drawdown is quite large at well P2-1, but the cause of this is not clear. The results show that the numerical model is able to identify the parameters at the site.

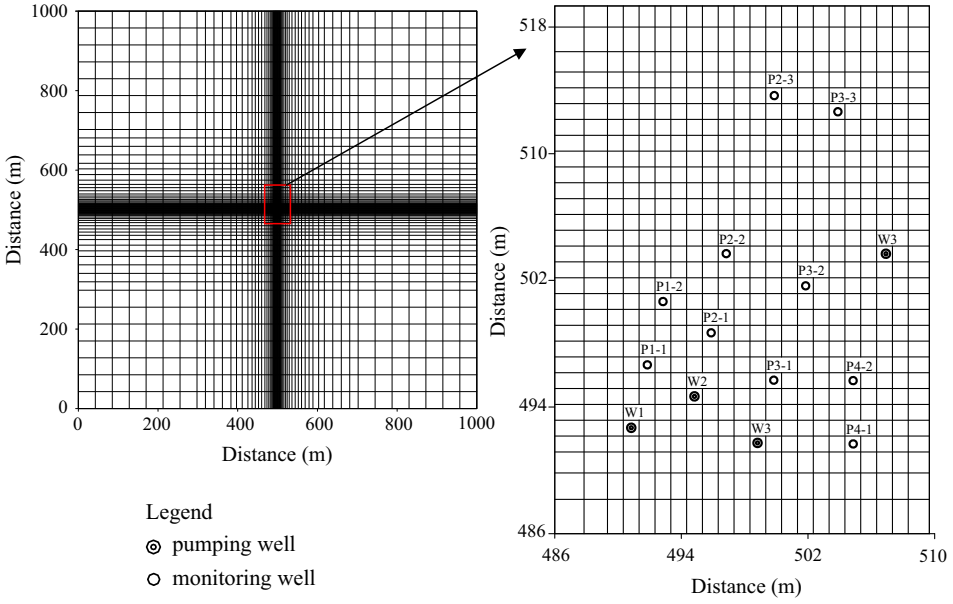

Fig. 11. Analysis range and mesh in plan.

Table 4
Soil layers and parameters used in the analysis.

Soil strata	Thickness (m)	k_h (m/d)	k_v (m/d)	S_s (m^{-1})
Backfill	2.6	4.00E−02	2.00E−02	1.50E−05
Silty clay	2.7	2.00E−02	6.70E−01	1.50E−05
Silt	7.3	6.00E−01	3.00E−01	1.00E−04
Silty clay	7.9	3.00E−02	1.00E−02	1.15E−05
Silt	4.1	3.00E−01	8.00E−02	2.30E−04
Silty sand	5.0	4.20E+00	1.50E+00	3.00E−04
Silt (see Fig. 12b)	5.0	3.00E−01	8.00E−02	2.30E−04
Silt	2.5	3.00E−01	8.00E−02	3.00E−04
Silty clay	3.9	2.00E−02	5.00E−03	3.00E−05
Silt	2.0	3.00E−01	8.00E−02	1.50E−04
Silty clay	6.8	2.00E−02	1.00E−02	1.60E−05
Silt	2.0	5.00E−01	2.00E−01	1.40E−04
Silty clay (see Fig. 12c)	2.0	2.00E−02	1.00E−02	1.60E−05
Silty clay	17.2	8.00E−04	5.00E−04	5.00E−06
Silty sand	4.0	3.80E+00	1.40E+00	1.00E−04
Silty clay	12.0	8.00E−04	5.00E−04	7.30E−06

Note: k_h = horizontal hydraulic conductivity; k_v = vertical hydraulic conductivity; S_s = specific storage.

Fig. 13 presents the contour of drawdown in Aq0, AqI, AqII and AqIII when the drawdown of each aquifer reached the maximum. The drawdown does not present concentric circles in AqI and AqII because the sand layer of AqI is disconnected with some silt and the silt layer of AqII is disconnected with some silty clay, which is shown in grey in Fig. 13. From Fig. 13, the maximum influential range of groundwater drawdown in Aq0 is 112 m; in AqI, it is 336 m; in AqII, it is 105 m; and in AqIII, it is 458 m, under the assumption of a drawdown of 0.1 m. The influential range decreases where the relative aquitard exists in AqI and AqII.

8. Discussion

8.1. Leakage effect of aquitards

In Fig. 6, there is drawdown in the upper aquifer during the pumping tests in Aq0, AqI and AqII, which indicates that there is a hydraulic connection between Aq0 and AqI and between AqI and AqII. The pumping test (see Fig. 6) in AqIII indicates that there is no hydraulic connection between AqII and AqIII. That is, the hydraulic conductivity of AdI and AdII is relatively high, and the permeability of AdIII is relatively low. The lack of leakage of AdIII indicates that the quality of bentonite clay ball seams for wells are sufficient. The numerical results show that the average horizontal hydraulic conductivity of silty clay in AdI and AdII is 0.03 m/d and 0.02 m/d, respectively. It is higher than that of Shanghai clay, which has the order of 10^{-5} m/d [24,44].

The leakage of aquitards has an effect on the drawdown of aquifers. This phenomenon is analysed using the FEM model. It is assumed that 4 wells at a depth of 30 m pump water from AqI for 30 days and that the discharge in each pumping well is 90 m^3/d. The four pumping wells are located in the four corners of a square that has sides of 20 m. Three monitoring wells are located in the middle of the square at depths of 13 m, 30 m and 48 m to observe the drawdown of Aq0, AqI and AqII. Let k_I be the hydraulic conductivity of AqI, and let k' be the hydraulic conductivity of silty clay in AdI and AdII. The ratio of hydraulic conductivity between the aquitards and aquifer I is defined as k'/k_I and is referred to as 'j'. Fig. 14 shows the relationship between the drawdown (s) of the aquifers and the ratio of hydraulic conductivity between the aquitards and aquifer I. In Fig. 14, with the exception of k', the parameters remain unchanged and the value of j varies from 0.0001 to 0.1. With an increase in the hydraulic conductivity of the aquitards, the drawdown of AqI decreases and the drawdown of Aq0 and AqII increases. When j is less than 0.014, the drawdown of Aq0 and AqII increases rapidly. When j is greater than 0.014, the drawdown of Aq0 and AqII increases slowly. In addition, because the thickness of AdI is less than that of AqII, the drawdown of Aq0 is greater than that of AqII. This result

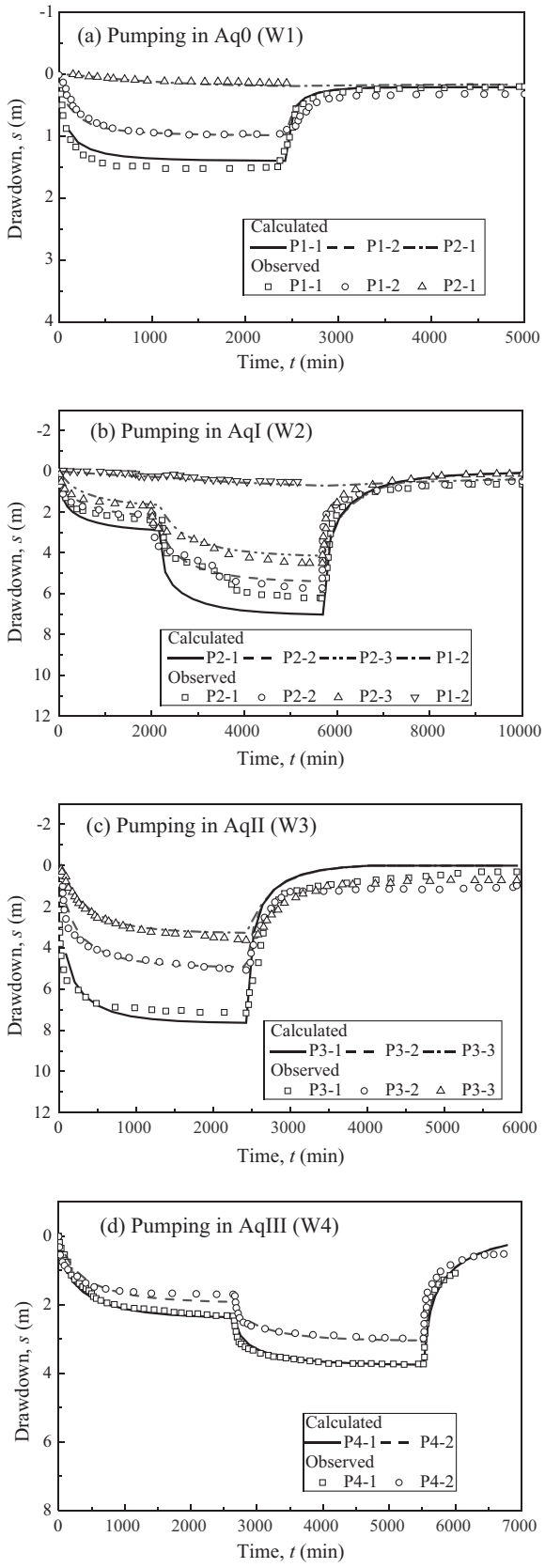

Fig. 12. Comparison between observed and calculated drawdown during the pumping test.

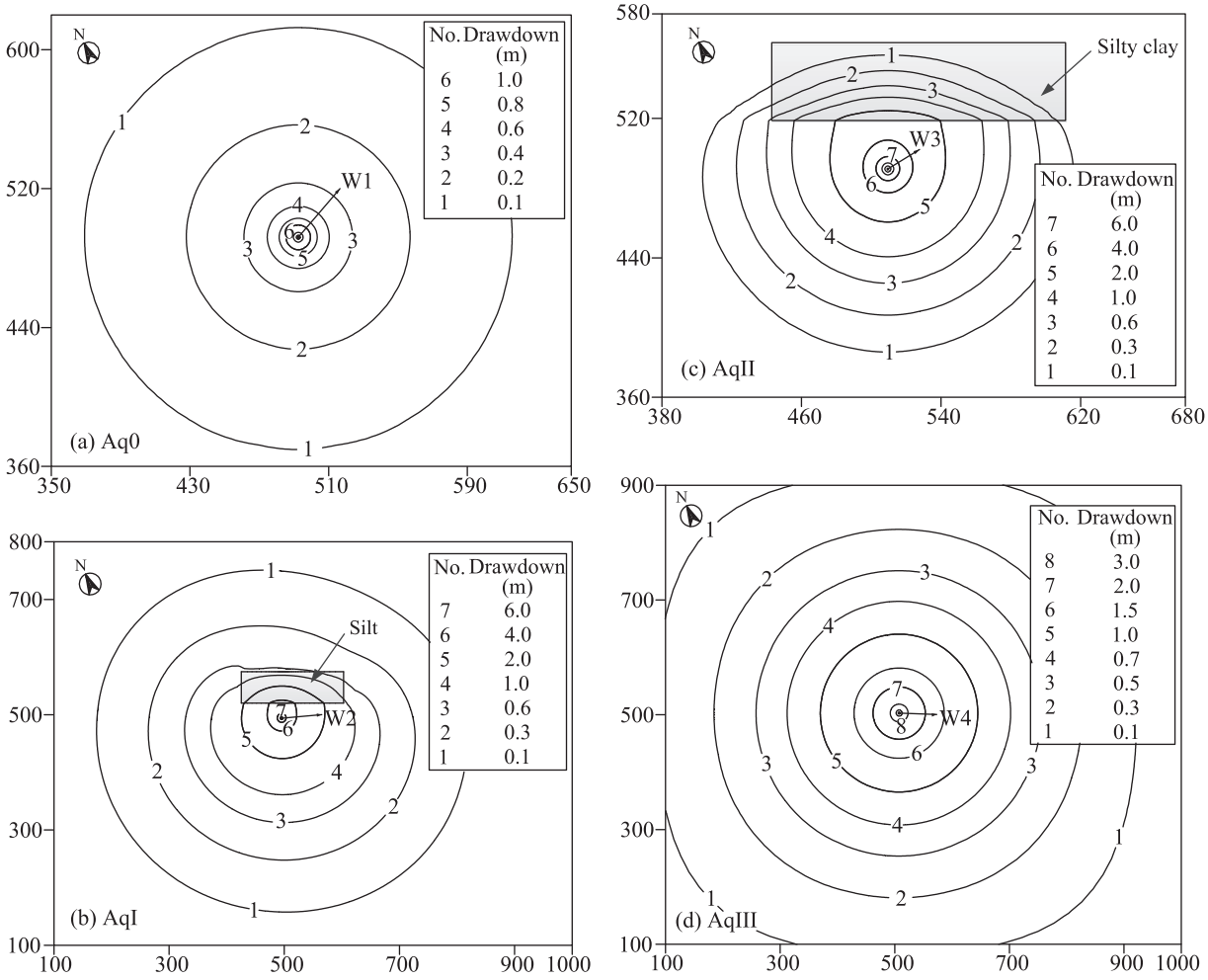

Fig. 13. Contour of drawdown.

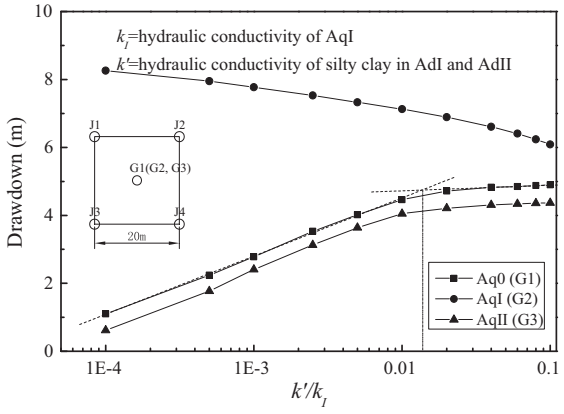

Fig. 14. Relationship between drawdown and the ratio of hydraulic conductivity between aquitards and aquifer I.

implies that the hydraulic conductivity of aquitards plays a significant role in the variation in the groundwater levels of aquifer systems during pumping.

8.2. Influence of wellbore storage

It can be observed from Fig. 8 that drawdown in the observational wells in the early stages diverges from the Cooper–Jacob curve. This phenomenon is caused by wellbore storage in the pumping wells. When pumping is performed in a large-diameter well, the initial groundwater extracted from the well is the water stored in the well casing. After this initial groundwater, the groundwater comes from the surrounding aquifers [9,21,31]. Therefore, drawdown in monitoring wells develops after a finite time. According to Papadopulos and Cooper [33] and Schafer [36], there is a critical time (t_c) for the wellbore storage effect. When the pumping time is greater than t_c, all of the drawdown points are located around the Cooper–Jacob curve, and the large-diameter well effect is negligible. In general, t_c increases with an increase of the radius of the pumping well. As observed in Fig. 8, if the internal radius of the pumping well is fixed, t_c increases with a decrease in the transmissivity of the confined aquifer.

8.3. Comparison between the analytical and numerical results

Tables 3 and 4 list the hydrogeological parameters of the four aquifers obtained using the analytical and numerical methods, respectively. The results show that the hydraulic conductivities of AqI, AqII, and AqIII calculated using the analytical method are higher than those calculated using the numerical method. This occurs because the Cooper–Jacob curve method is based on the following assumptions: (i) the confined aquifer is homogeneous, isotropic, and of uniform thickness over the area influenced by pumping, (ii) the well diameter is small and well storage is negligible, and (iii) confined aquifers are always entirely isolated from

above water sources [14,21]. In this situation, for example, when pumping is performed in AqI, there is leakage from adjacent aquifers, which leads to a higher result than the actual value. Moreover, the storage coefficient calculated from the Cooper–Jacob curve method can be influenced by wellbore storage, particularly for early-time drawdown data [9,17]. The analytic calculation is based on the data obtained from the middle to the later stages of the pumping tests such that the error caused by the influence of wellbore storage is relatively small. The three-dimensional numerical method considers aquifers and aquitards to be a unified hydrogeological model. The back calculation is performed throughout the process of the pumping tests, and the hydrogeological parameters of all soils can be calculated. For hydraulic conductivity, values can be obtained for both the horizontal and vertical directions. Thus, the values obtained from the numerical method are closer to the actual values than those obtained from the analytical method.

9. Concluding remarks

To investigate the hydrogeological characteristics of aquifers in the construction site, four sets of single-well pumping tests were performed near the excavation pit, and analytical methods and numerical simulation were used to analyse the test results. The following conclusions can be drawn from the pumping tests and analyses for this case study:

(1) The pumping test results indicate that there is a hydraulic connection between Aq0 and AqI and between AqI and AqII, and the hydraulic connection between AqI and AqII is poorer than that between AqI and Aq0. There is no hydraulic connection between AqII and AqIII. These results show that AdI has the highest leakage effect, AdII has the second highest effect, and AdIII has no leakage effect. Thus, the leakage effect of the aquitards (AdI and AdII) plays a significant role in the variation of the groundwater level of multi-aquifer systems during pumping tests.

(2) The value of the hydraulic conductivity of Aq0 is calculated using the Dupuit equation, and the values of the hydraulic conductivity, transmissivity and storage coefficient of AqI, AqII and AqIII are estimated using the Cooper–Jacob method. The hydraulic conductivity of Aq0 is 0.44 m/d. The values of the hydraulic conductivity, transmissivity and storage coefficient of AqI are 4.94 m/d, 24.71 m^2/d and 6.89×10^{-4}, respectively. For AqII, they are 1.38 m/d, 2.76 m^2/d and 2.11×10^{-4}, respectively, and for AqIII, they are 3.84 m/d, 19.35 m^2/d and 3.00×10^{-4}, respectively.

(3) The values of the influence radius calculated by the approximate method are 48 m for W1 in Aq0 and 18 m, 20 m and 72 m for W4 in AqIII. The values calculated by the graphical method are 220 m and 480 m for W2 in AqI and 95 m for W3 in AqII.

(4) A numerical model to simulate the field pumping tests based on the FEM is established. The calculated value of the groundwater head using the model matched the measured value. The values of the horizontal hydraulic conductivity (k_h), vertical hydraulic conductivity (k_v) and specific storage (S_s) of each layer are obtained by back calculation based on the test results.

(5) The values of the hydraulic conductivity of AqI, AqII and AqIII from the Cooper–Jacob method are higher than those from the numerical simulation due to the leakage of AdI and AdII. The hydraulic conductivity of the aquitards and the radius of the well have an effect on the calculated parameters obtained from the Cooper–Jacob method. The computing deviation increases with an increase in the hydraulic conductivity of the aquitards and the radius of the well. To reduce the computing error caused by the wellbore storage effect, the pumping time should be sufficiently long, and the data obtained from the middle to later stages should be used to calculate parameters. In this field case, the drawdown in the observational wells is influenced by the well storage within the first 100–200 min; thus, the time duration in the pumping test should be more than 2000 min to obtain accurate parameters.

(6) Compared with the analytical method, the numerical method obtained more reliable results. The numerical method can provide parameters not only for the pumping aquifer but also for other layers. It is suggested that the numerical method be used to obtain the hydrological parameters in the following situations: (i) where pumping is performed in an aquifer and groundwater variation of the other layers is observed; (ii) where leakage from the aquitards is serious; and (iii) where the geological conditions are very complicated, for example, when the thickness of the aquifer is not uniform and the continuity of the aquifer is not consistent in the horizontal direction.

Acknowledgements

The research work described herein was funded by the National Nature Science Foundation of China (NSFC) (Grant No. 41472252) and also partially supported by the National Basic Research Program of China (973 Program: 2015CB057806). This financial support is gratefully acknowledged.

References

[1] Bear J. Dynamics of fluids in porous media. American Elsevier Publishing Company, INC.; 1972.
[2] Bear J. Hydraulics of groundwater. New York: McGraw-Hill; 1979.
[3] Çimen M. Confined aquifer parameters evaluation by slope-matching method. J Hydrol Eng 2008;13(3):141–5.
[4] Chai J-C, Shen S-L, Zhu H-H, Zhang X-L. Land subsidence due to groundwater drawdown in Shanghai. Géotechnique 2004;54(2):143–7.
[5] Chai J-C, Horpibulsuk S, Shen S-L, Cater JP. Consolidation analysis of clayey deposit under vacuum pressure with horizontal drains. Geotext Geomembranes 2014;42(5):437–44.
[6] Chai J-C, Hossain MJ, Cater JP, Shen S-L. Cone penetration-induced pore pressure distribution and dissipation. Comput Geotech 2014;2014(57):105–13.
[7] Chai J-C, Shen S-L, Ding W-Q, Zhu H-H, Cater JP. Numerical investigation of the failure of a building in Shanghai, China. Comput Geotech 2014;55(2014):482–93.
[8] Chapuis RP. Similarity of internal stability criteria for granular soils. Can Geotech J 1992;29(4):711–3.
[9] Chapuis RP, Chenaf D. Slug tests in a confined aquifer: experimental results in a large soil tank and numerical modelling. Can Geotech J 2002;39(1):14–21.
[10] Chapuis RP, Aubertin M. On the use of the Kozeny-Carman equation to predict the hydraulic conductivity of soils. Can Geotech J 2003;40:616–28.
[11] Chapuis RP, Chenaf D. Effects of monitoring and pumping well pipe capacities during pumping tests in confined aquifers. Can Geotech J 2003;40(6):1093–103.
[12] Chapuis RP. Predicting the saturated hydraulic conductivity of sand and gravel using effective diameter and void ratio. Can Geotech J 2004;41:787–95.
[13] Chapuis RP, Dallaire V, Marcotte D, Chouteau M, Acevedo N, Gagnon F. Evaluating the hydraulic conductivity at three different scales within an unconfined sand aquifer at Lachenaie, Quebec. Can Geotech J 2005;42(4):1212–20.
[14] Cooper HH, Jacob CE. A generalized graphical method for evaluating formation constants and summarizing well field history. Trans Am Geophys Union 1946;27(4):526–34.
[15] Dupuit J. Études théoriques et pratiques sur le movement des eaux dans les canaux découverts et à travers les terrains perméables. 2nd ed. Paris: Dunod; 1863. p. 229–93.
[16] Jean JS. Pumping testing using a siphon well. Water Resour Manage 1996;10(2):81–105.
[17] Jiao JJ, Rushton KR. Sensitivity of drawdown to parameters and its influence on parameter estimation for pumping tests in large-diameter wells. Ground Water 1995;33(5):794–800.

[18] Jiao JJ. Investigation of extra recharge during pumping in Nottingham aquifer. Ground Water 1996;34(5):795–800.
[19] Jiao JJ, Zheng C. The different characteristics of aquifer parameters and their implications on pumping-test analysis. Ground Water 1997;35(1):25–9.
[20] Johnson GS, Frederick DB, Cosgrove DM. Evaluation of a pumping test of the Snake River Plain aquifer using axial-flow numerical modeling. Hydrogeol J 2002;10(3):428–37.
[21] Kruseman GP, de Ridder NA. Analysis and evaluation of pumping test data. Wageningen: International Institute for Land Reclamation and Improvement; 1994.
[22] Kuang X, Jiao JJ, Zhang K, Mao D. Air and water flows induced by pumping tests in unconfined aquifers with low-permeability zones. Hydrol Process 2014;28(21):5450–64.
[23] Lin H-T, Tan Y-C, Chen C-H, Yu H-L, Wu S-C, Ke K-Y. Estimation of effective hydrogeological parameters in heterogeneous and anisotropic aquifers. J Hydrol 2010;389(1):57–68.
[24] Luo Z-J, Zhang Y-Y, Wu Y-X. Finite element numerical simulation of three-dimensional seepage control for deep foundation pit dewatering. J Hydrodyn 2008;20(5):596–602.
[25] Ma L, Xu Y-S, Shen S-L, Sun W-J. Evaluation of the hydraulic conductivity of aquifers with piles. Hydrogeol J 2014;22(2):371–82.
[26] Masrouri F, Bicalho KV, Kawai K. Laboratory hydraulic testing in unsaturated soils. In: Laboratory and Field Testing of Unsaturated Soils. Netherlands: Springer; 2009. p. 79–92.
[27] Majumdar PK, Sekhar M, Sridharan K, Mishra GC. Numerical simulation of groundwater flow with gradually increasing heterogeneity due to clogging. J Irrig Drain Eng 2008;134(3):400–4.
[28] Mbonimpa M, Aubertin M, Chapuis RP, Bussière B. Practical pedotransfer functions for estimating the saturated hydraulic conductivity. Geotech Geol Eng 2002;20(3):235–59.
[29] Ministry of Construction of the People's Republic of China (MCPRC). Technical standard for water-supply well. GB 50296-99. Beijing: China Architecture & Building Press; 1999 [in Chinese].
[30] Ministry of Construction of the People's Republic of China (MCPRC). Standard for hydrogeological investigation of water-supply. GB 50027-2001. Beijing: China Architecture & Building Press; 2001 [in Chinese].
[31] Ni JC, Cheng W-C, Ge L. A case history of field pumping tests in a deep gravel formation in the Taipei Basin, Taiwan. Eng Geol 2011;117(1):17–28.
[32] Ou C-Y, Chen S-H. Performance and analysis of pumping tests in a gravel formation. Bull Eng Geol Environ 2010;69(1):1–12.
[33] Papadopulos IS, Cooper HH. Drawdown in a well of large diameter well. Water Resour Res 1967;3:241–4.
[34] Pickles AR, Lee SW, Norcliffe BAW. Groundwater and ground movement around deep excavation. Geotech Eng 2003;156(3):147–58.
[35] Roy D, Robinson KE. Surface settlements at a soft soil site due to bedrock dewatering. Eng Geol 2009;107(3):109–17.
[36] Schafer DC. Casing storage can affect pumping test data. Johnson Drillers' Journal, Jan/Feb. St. Paul, Minnesota: Johnson Division, UOP Inc.; 1978.
[37] Sethi R. A dual-well step drawdown method for the estimation of linear and non-linear flow parameters and wellbore skin factor in confined aquifer systems. J Hydrol 2011;400(1):187–94.
[38] Shaqour FM, Hasan SE. Groundwater control for construction purposes: a case study from Kuwait. Environ Geol 2008;53(8):1603–12.
[39] Shen S-L, Han J, Huang X-C, Du S-J. Laboratory studies on property changes in surrounding clays due to installation of deep mixing columns. Mar Georesour Geotechnol 2003;21(1):15–35.
[40] Shen S-L, Xu Y-S, Hong Z-S. Estimation of land subsidence based on groundwater flow model. Mar Georesour Geotechnol 2006;24(2):149–67.
[41] Shen S-L, Xu Y-S. Numerical evaluation of land subsidence induced by groundwater pumping in Shanghai. Can Geotech J 2011;48(9):1378–92.
[42] Shen S-L, Wu H-N, Cui Y-J, Yin Z-Y. Long-term settlement behaviour of metro tunnels in the soft deposits of Shanghai. Tunn Undergr Space Technol 2014;40(1):309–23.
[43] Theis CV. The relation between the lowering of the piezometric surface and the rate and duration of discharge of a well using groundwater storage. Eos Trans AGU 1935;16:519–24.
[44] Tan Y, Wang D-L. Characteristics of a large-scale deep foundation pit excavated by central-island technique in Shanghai soft clay. I: bottom-up construction of the central cylindrical shaft. J Geotech Geoenviron 2013;139(11):1875–93.
[45] Vilarrasa V, Carrera J, Jurado A, Pujades E, Vázquez-Suné E. A methodology for characterizing the hydraulic effectiveness of an annular low-permeability barrier. Eng Geol 2011;120(1):68–80.
[46] Wang J-X, Hu L-S, Wu L-G, Tang Y-Q, Zhu Y-F, Yang P. Hydraulic barrier function of the underground continuous concrete wall in the pit of subway station and its optimization. Environ Geol 2009;57(2):447–53.
[47] Xu Y-S, Shen S-L, Du Y-J. Geological and hydrogeological environment in Shanghai with geohazards to construction and maintenance of infrastructures. Eng Geol 2009;109(3–4):241–54.
[48] Xu Y-S, Ma L, Du Y-J, Shen S-L. Analysis on urbanization induced land subsidence in Shanghai. Nat Hazards 2012;63(2):1255–67.
[49] Xu Y-S, Ma L, Shen S-L, Sun W. Evaluation of land subsidence by considering underground structures that penetrate the aquifers of Shanghai, China. Hydrogeol J 2012;20(8):1623–34.
[50] Xu Y-S, Shen S-L, Ma L, Sun W-J, Yin Z-Y. Evaluation of the blocking effect of retaining walls on groundwater seepage in aquifers with different insertion depths. Eng Geol 2014;183:254–64.
[51] Yang J-M, Zheng G, Jiao Y. Test and analysis of the aquifer at Tianjin station. China Civ Eng J 2008;41(7):67–70 [in Chinese].
[52] Yin J-H. Non-linear creep of soils in oedometer tests. Géotechnique 1999;49(5):699–707.
[53] Yin J-H, Graham J. Elastic visco-plastic modelling of the time-dependent stress-strain behavior of soils. Can Geotech J 1999;36(4):736–45.
[54] Yin Z-Y, Karstunen M, Chang C-S, Koskinen M, Lojander M. Modeling time-dependent behavior of soft sensitive clay. J Geotech Geoenviron ASCE 2011;137(11):1103–13.
[55] Yin Z-Y, Chang C-S. Stress-dilatancy behavior for sand under loading and unloading conditions. J Numer Anal Methods Geomech 2013;37(8):855–70.
[56] Zeng L-L, Hong Z-S, Cai Y-Q, Han J. Change of hydraulic conductivity during compression of undisturbed and remolded clays. Appl Clay Sci 2011;51(1–2):86–93.